



On the Possible Coordination on a ^3MC State Itself? Mechanistic Investigation Using DFT-Based Methods

Adrien Soupart, Fabienne Alary, Jean-Louis Heully and Isabelle M. Dixon * 

Laboratoire de Chimie et Physique Quantiques, UMR 5626 CNRS/Université Toulouse 3-Paul Sabatier, Université de Toulouse, 118 route de Narbonne, 31062 Toulouse, France; adrien.soupart@irsamc.ups-tlse.fr (A.S.); fabienne.alary@irsamc.ups-tlse.fr (F.A.); jean-louis.heully@irsamc.ups-tlse.fr (J.-L.H.)

* Correspondence: isabelle.dixon@irsamc.ups-tlse.fr

Received: 30 January 2020; Accepted: 16 February 2020; Published: 19 February 2020



Abstract: Understanding light-induced ligand exchange processes is key to the design of efficient light-releasing prodrugs or photochemically driven functional molecules. Previous mechanistic investigations had highlighted the pivotal role of metal-centered (MC) excited states in the initial ligand loss step. The question remains whether they are equally important in the subsequent ligand capture step. This article reports the mechanistic study of direct acetonitrile coordination onto a ^3MC state of $[\text{Ru}(\text{bpy})_3]^{2+}$, leading to $[\text{Ru}(\text{bpy})_2(\kappa^1\text{-bpy})(\text{NCMe})]^{2+}$ in a $^3\text{MLCT}$ (metal-to-ligand charge transfer) state. Coordination of MeCN is indeed accompanied by the decoordination of one pyridine ring of a bpy ligand. As estimated from Nudged Elastic Band calculations, the energy barrier along the minimum energy path is 20 kcal/mol. Interestingly, the orbital analysis conducted along the reaction path has shown that creation of the metallic vacancy can be achieved by reverting the energetic ordering of key $\text{d}\sigma^*$ and bpy-based π^* orbitals, resulting in the change of electronic configuration from ^3MC to $^3\text{MLCT}$. The approach of the NCMe lone pair contributes to destabilizing the $\text{d}\sigma^*$ orbital by electrostatic repulsion.

Keywords: ruthenium polypyridine complex; photochemistry; photosolvolytic mechanism; metal-centered excited states; triplet state reactivity; nudged elastic band; DFT; molecular orbitals

1. Introduction

The photophysics of ruthenium polypyridine compounds is governed by the subtle balance between the population of two types of triplet excited states of similar energies: metal-to-ligand charge transfer states (MLCT) and metal-centered states (MC) [1]. $^3\text{MLCT}$ states are photoluminescent, contrary to ^3MC states, which quench the luminescence and may lead to ligand loss [2]. Forty years of spectroscopic studies on this family of compounds have provided a wealth of robust experimental data, but MC states are spectroscopically “dark” and therefore their theoretical characterization is essential in the rationalization and the anticipation of photophysical properties. For more than a decade, we have been able to optimize ^3MC excited states [3] and to explore the topology of the lowest triplet potential energy surface using DFT-based methods [4–9]. Spectacular bond elongations and angular distortions have been characterized in numerous Ru(II) ^3MC states [10–28] and for other metals, e.g., Ir(III) [29–31]. Our contribution to the field covers photoisomerization mechanisms [32–34] and photoluminescence quenching mechanisms [35,36], as well as exploratory ruthenium(II) [37,38] and iron(II) [39–42] photophysics, in a constant dialogue with experimental chemists.

In the course of our theoretical investigations of photosubstitution mechanisms, we have identified some key ^3MC states along the pathways for ligand photorelease, particularly pentacoordinate or pseudopentacoordinate species [7,8]. In that work, these ^3MC states have been considered to be involved in such mechanisms via intersystem crossing (ISC) through a neighboring minimum energy

crossing point (MECP), allowing the system to populate an electrophilic, coordinatively unsaturated, and closed-shell species. The final coordination of a molecule of incoming ligand is thought to be an efficient process [43–47] and yields a κ^1 -bound intermediate product that requires the absorption of a second photon to fully release the departing bidentate ligand [48,49]. However an alternative pathway can also be envisaged, overall requiring only one photon, namely the direct reaction between the incoming ligand and the complex in its distorted ^3MC state, to form a new complex with triplet spin multiplicity according to Wigner rules. The aim of this work was therefore to investigate this type of reactivity through DFT-based methods, computing minimum energy paths using Nudged Elastic Band calculations and undertaking a thorough orbital analysis along this path. The model reaction we chose is the approach of an acetonitrile molecule on the previously reported $^3\text{MC}_{\text{cis}}$ state of $\text{Ru}(\text{bpy})_3^{2+}$ [50]. This state, repelling the two pyridine fragments of a single bpy ligand, is thought to be prone to bpy loss, or at least more prone than the classical $^3\text{MC}_{\text{trans}}$ state that repels two pyridines from two different ligands (Figure 1).

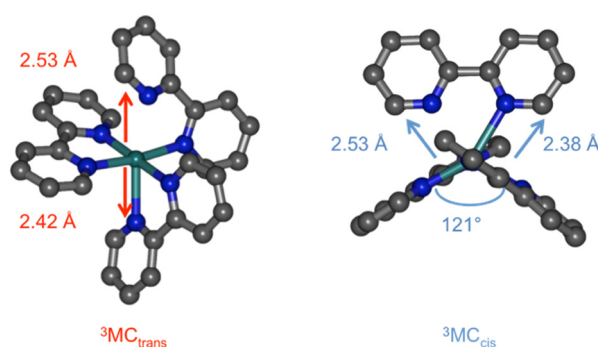
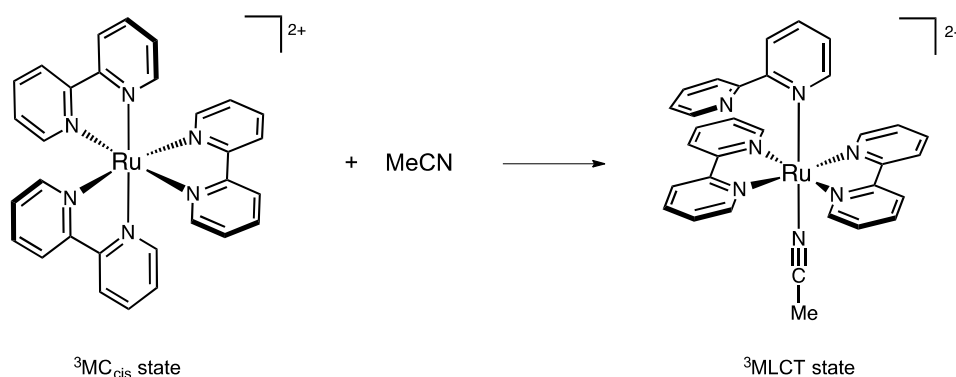


Figure 1. Structures of $^3\text{MC}_{\text{trans}}$ and $^3\text{MC}_{\text{cis}}$ in $\text{Ru}(\text{bpy})_3^{2+}$ (H atoms not shown).

Acetonitrile was selected for its charge neutrality, for being a reactant that bears only one lone pair, and for being an aprotic and weakly self-associating solvent, that allows us to consider the approach of a single NCMe molecule as a reasonable model. The aim of this work was to envisage direct NCMe coordination on the $^3\text{MC}_{\text{cis}}$ state of $\text{Ru}(\text{bpy})_3^{2+}$ in order to form an intermediate triplet state bearing one monodentate bpy and one bound acetonitrile ligand (Scheme 1). This process was found to have an energy barrier of 20 kcal/mol. Analysis of the coordination process from an orbital perspective has shown that MeCN approach and change in electronic configuration from ^3MC to $^3\text{MLCT}$ were intimately related.



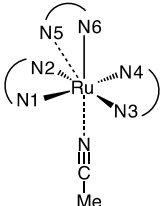
Scheme 1. Coordination of one acetonitrile molecule onto the $^3\text{MC}_{\text{cis}}$ state of $\text{Ru}(\text{bpy})_3^{2+}$.

2. Results and Discussion

Working on the photoinduced loss of bidentate ligands, Elliott et al. reported the crystallographic characterization of intermediate photoproducts of the type *trans*-[Ru(bpy)(κ^2 -btz)(κ^1 -btz)(NCMe)]²⁺ bearing a singly-bound bitriazolyl (btz) ligand [48,49]. By analogy we have built and optimized *trans*-[Ru(bpy)₂(κ^1 -bpy)(NCMe)]²⁺ in a singlet state, from which an excited state with triplet spin multiplicity was subsequently optimized by unrestricted DFT. This state is unambiguously of MLCT electronic nature and was used as endpoint for a minimum energy path calculation. This state contains a bpy ligand that is a monodentate, κ^1 -bpy ligand. The exploration of the envisaged chemical reaction was undertaken starting from the ³MC_{cis} state having an acetonitrile molecule 5 Å away with its lone pair oriented towards the metal, in the most open quadrant of the complex. Note that NCMe is not interacting with the [Ru(bpy)₃]²⁺ moiety in this structure, as estimated from its total energy that is equal to the sum of the fragments' energies.

At the starting point of the reaction path the complex is in the ³MC_{cis} state. The rationale for this choice lies in its presumed higher propensity for ligand loss than the ³MC_{trans} state. This is due to its peculiar geometry repelling a single bpy ligand and opening a quadrant, allowing a potentially entering ligand to approach the metal [50]. In the ³MC_{cis} state, two major elongations are found towards the same bpy ligand (Ru–N5 and Ru–N6, Table 1), the opposite quadrant opens up to 121° (Figure 1), and the Mulliken spin population on ruthenium is 1.7. At the end point, the complex contains one monodentate bpy ligand (the pyridine ring containing N5 is rotated out of plane and Ru–N5 = 3.59 Å); the Ru–N6 distance is standard and the two bonds towards the formally anionic bpy ligand are the shortest (Ru–N3 and Ru–N4). The ³MLCT nature of this state is illustrated by its Mulliken spin population on ruthenium, which is 0.9 (the other spin residing on a bpy ligand).

Table 1. Atom numbering and Ru–N distances (Å) at the start (³MC + MeCN) and end (³MLCT) points of the computed reaction path.

	Ru–N	³ MC + MeCN	³ MLCT
	Ru–N1	2.135	2.118
	Ru–N2	2.080	2.110
	Ru–N3	2.078	2.049
	Ru–N4	2.177	2.057
	Ru–N5	2.530	3.593
	Ru–N6	2.384	2.132
	Ru–NCMe	5.000	2.055

Minimum energy paths (MEPs) can be efficiently computed using the Nudged Elastic Band method [51,52], which discretizes the reaction path into a series of points, called beads. The initial path consists in a series of single point energy calculations along a geometry interpolation, which we perform using the image dependent pair potential (IDPP) method [53]. Subsequently each intermediate bead is minimized using path gradient and tangent information, until convergence to the MEP. The energy gap between the two endpoints is 17 kcal/mol, and a first estimate of the energy barrier for the reaction is 18 kcal/mol, as shown on Figure 2. The energy profile for this reaction appears as having a very moderate slope up to bead 15 (Ru–NCMe distance of 2.77 Å), after which the energy suddenly rises by about 14 kcal/mol at bead 18.

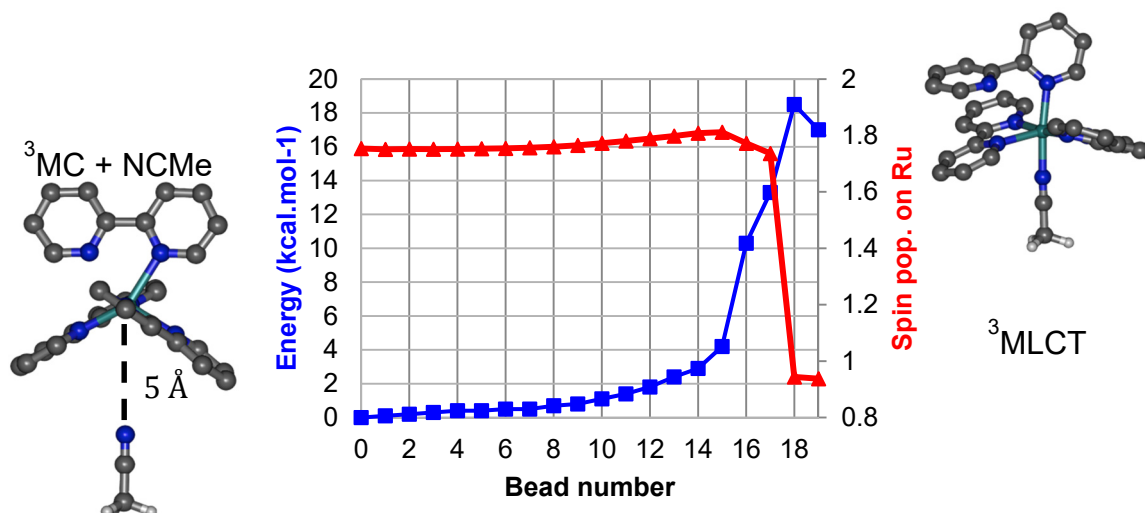


Figure 2. Minimum energy path (blue) and Mulliken spin population on Ru (red) for the coordination of acetonitrile on the ^3MC state from Nudged Elastic Band calculations.

A sudden drop in the Mulliken spin population on ruthenium is apparent between bead 17 and bead 18, signifying a change between MC and MLCT character. Thus, a second nudged elastic band (NEB) calculation was performed to refine this region. For simplicity the beads in this second calculation have been numbered with intermediate values 17.25, 17.50, and 17.75 (Figure 3).

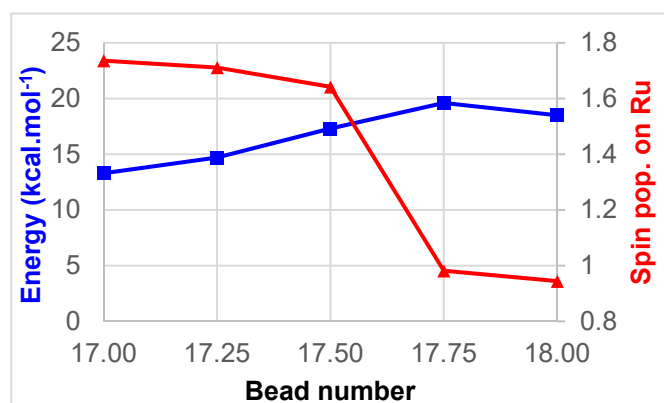


Figure 3. Minimum energy path (blue) and Mulliken spin population on Ru (red) between beads 17 and 18 of the reaction path.

The switch between MC and MLCT states here occurs between beads 17.50 and 17.75, providing a refined energy barrier of 20 kcal/mol. Wiberg bond indices (WBIs) have been computed at all geometries along the reaction path, and have been used to quantify the Ru–N interactions. In the starting ^3MC structure, two Ru–N bonds are significantly elongated as a result of the population of an antibonding $\text{d}\sigma^*$ orbital, namely Ru–N5 (2.53 Å) and Ru–N6 (2.38 Å). The corresponding WBIs are consequently the lowest, 0.19 and 0.26 respectively (Figure 4). Bonds *trans* to these, Ru–N4 and Ru–N1, are slightly elongated with WBIs of 0.36 and 0.41. The two remaining bonds, Ru–N2 and Ru–N3, display WBIs that are similar to the ones found in the ground state, i.e., 0.44. Notably the gradual drop in the Ru–N5 WBI along the reaction path is paralleled by a gradual increase in the Ru–NCMe WBI, until bead 17.50 where this latter WBI doubles to reach 0.45 in the $^3\text{MLCT}$ state. At the endpoint, the highest two WBIs are the ones to the nitrogen atoms of the formally anionic bpy ligand, N3 (0.51) and N4 (0.54), Ru–N3, and Ru–N4 being the shortest bonds (Table 1). The intermediate zone (between beads 7–14), where WBIs towards departing and incoming ligands are both low, illustrates the fact that the complex gets pentacoordinated and is stabilized by two successive weak Ru–N interactions along this path.

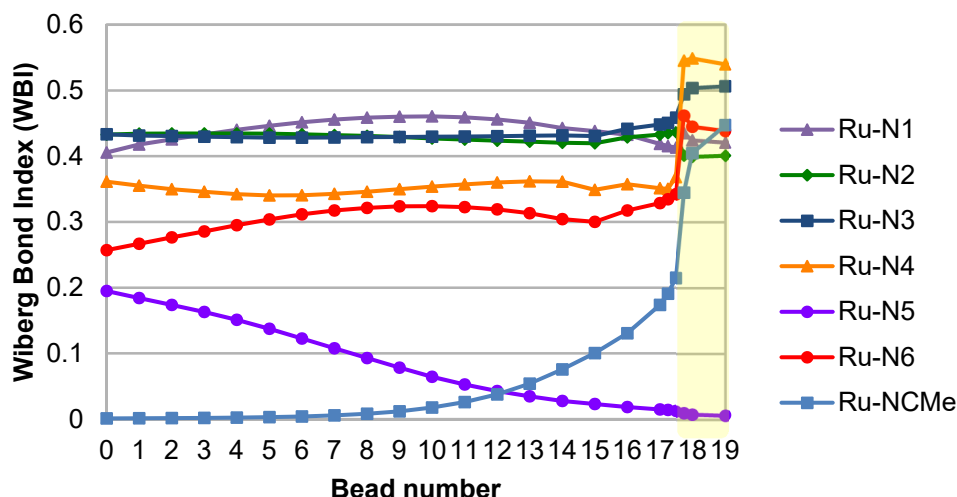


Figure 4. Evolution of WBIs along the reaction path. The MC–MLCT transition region is highlighted in yellow.

In order to allow the Ru–NCMe bond to form, a low-lying vacancy should be identified on the metal with appropriate symmetry and orientation to enable significant overlap with the incoming nitrogen lone pair. The crucial orbitals in this process are thus: (i) the metallic $d\sigma^*$ orbitals, (ii) the NCMe lone pair that eventually evolves to a Ru–NCMe dative bond, and (iii) the bpy-based π^* orbital that will be singly occupied in the final $^3\text{MLCT}$ state. The eigenvalues of these four molecular orbitals (MOs) are plotted against bead number on Figure 5. All lines are broken between beads 17.50 and 17.75 to signify the rupture in the correlation diagram, e.g., when the NCMe lone pair is replaced by a bonding Ru–NCMe interaction. At this very point along the path, we propose that the electrostatic repulsion between the NCMe lone pair and the singly occupied $d\sigma^*1$ orbital (as illustrated by the gradual destabilization of $d\sigma^*1$ from bead 12 onwards) is such that the $d\sigma^*1$ is destabilized to a point where its energy is higher than that of the bpy π^* orbital. As a result, the electron that was in $d\sigma^*1$ in the MC state is transferred to the bpy π^* orbital, thus producing an MLCT state. This change in electronic configuration is what allows the total energy of the system to decrease towards the endpoint of the path. In addition, the quasi invariance in the energy of $d\sigma^*2$ confirms that it is always nonbonding towards the incoming ligand.

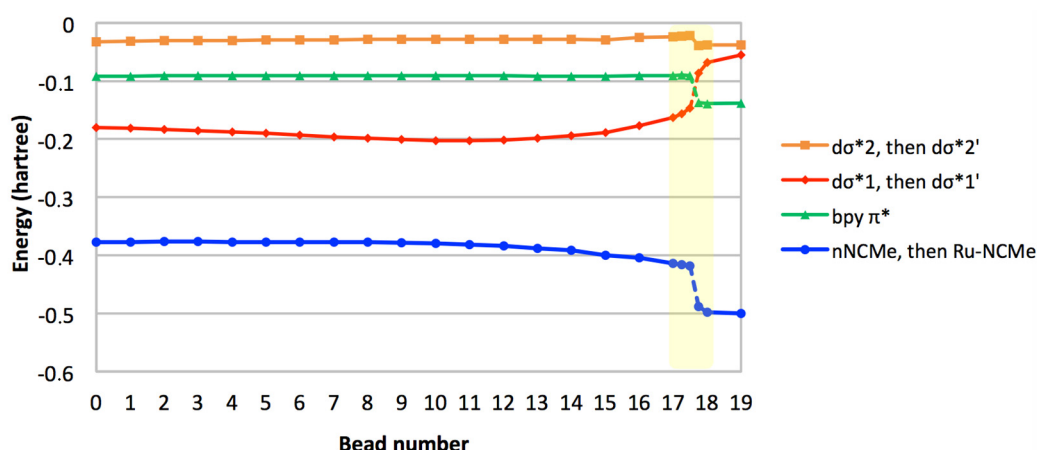


Figure 5. Selected orbital eigenvalues along the reaction path. The MC–MLCT transition region is highlighted in yellow.

A close inspection of these crucial orbitals, at beads 17.50 and 17.75 (Figure 6), reveals that the formation of the Ru–NCMe bond is accompanied by a repolarization of both $d\sigma^*$ orbitals, as seen for

instance in the disappearance of the Ru–N6 antibonding interaction in $d\sigma^*2'$. The interaction of $d\sigma^*1$ with the NCMe lone pair produces two new orbitals: the Ru–NCMe bond and the $d\sigma^*1'$ antibond (Figure S1). In this system, coordination of the incoming ligand is accompanied by the change of electronic state nature, from 3MC to 3MLCT , which has a vacant $d\sigma^*1'$ (as stated in the introduction, an alternative to create a metallic vacancy is spin crossing to a closed-shell pentacoordinate singlet state [8,54], which would also vacate the required $d\sigma^*$ orbital).

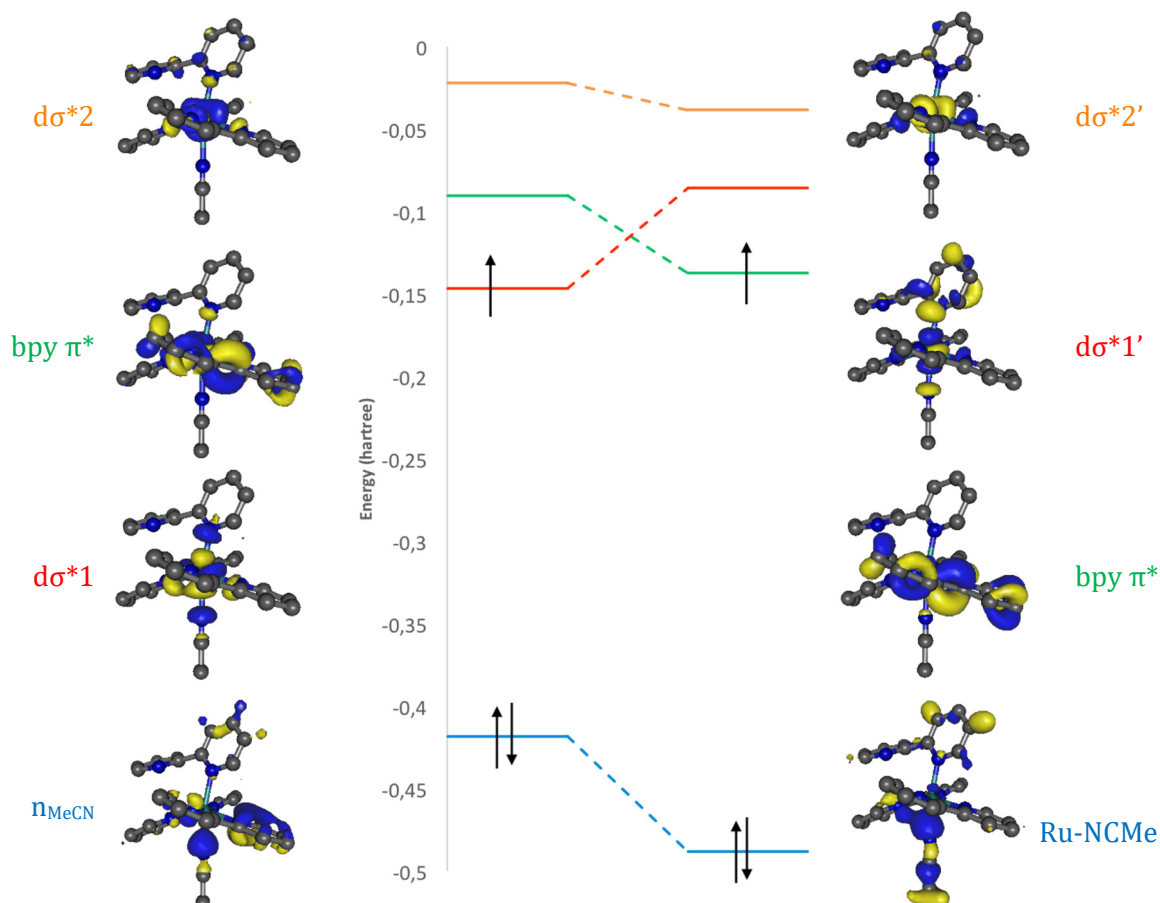


Figure 6. Partial MO correlation diagram between beads 17.50 and 17.75 (Kohn–Sham orbitals), showing NCMe coordination at bead 17.75 (a more complete MO diagram is given as Figure S2).

3. Computational Details and Methods

Geometry optimizations were performed without symmetry with Orca [55] using the B3LYP functional [56,57], a relativistic small core pseudopotential on Ru (SD28) [58], the def2-TZVP(-f) basis set [59], and the empirical D3 dispersion correction [60,61]. Solvent effects were modelled as the SMD polarizable continuum [62]. The restricted Kohn–Sham formalism was used for ground states, while its unrestricted analogue was used for triplet states. SCF convergence was achieved using the DIIS algorithm followed by a semi-quadratic SOSCF converger. Frequency calculations were run at the same level of theory and the absence of imaginary frequencies ascertained the nature of these points as minima. Molecular orbitals were viewed using Gabedit [63]. Mulliken spin densities on Ru were used as a straightforward descriptor of the electronic nature of the triplet excited state (~ 0.9 for a 3MLCT state, ~ 1.8 for a 3MC state). Orbital analysis was systematically undertaken to view the localization of the unpaired electrons.

The 3MLCT – 3MC minimum energy paths were optimized with the nudged elastic band (NEB) method [51,52] using a python module developed in the Clancy group [64] that is interfaced with Orca. The convergence criterion was set to 0.03 eV/Å. A 20-frame initial path was prepared by interpolating

start and end geometries using the IDPP method [53]. The geometries were previously processed using lab-developed programs to minimize the discrepancy between start and end geometries. These calculations were performed at the same level of theory as all the geometry optimizations. Convergence of the MEP was achieved using a combination of FIRE and BFGS algorithms.

4. Conclusions

In this work, we have envisaged the direct addition of an acetonitrile molecule on the $^3\text{MC}_{\text{cis}}$ state of $[\text{Ru}(\text{bpy})_3]^{2+}$, a state that we had proposed to consider as potentially photoreactive [50]. Nudged elastic band calculations have provided an energy barrier of 20 kcal/mol for this model reaction, significantly higher than the energy barrier involved in the spin crossing process towards a pentacoordinate ground state species [54] (note that the former pathway requires a single photon excitation, whereas the latter requires a second photon to fully release the departing bidentate ligand). The orbital analysis we have conducted along the reaction path has enabled us to describe the chemical reaction and the MC–MLCT transition. The change in electronic nature, from ^3MC to $^3\text{MLCT}$, is concomitant to the approach of the NCMe lone pair and triggers the interaction between the newly formed metallic vacancy and the NCMe lone pair. In this view, the ^3MC state itself can be seen as unable to bind MeCN. It is noteworthy that the approach of an incoming nucleophile is able to perturbate the metal complex so as to modify the electronic nature of its excited state. These results offer an interesting glimpse of processes that could be involved in excited state reaction mechanisms under specific experimental conditions such as pulsed irradiation. We are currently extending this work to the mechanistic study of the subsequent steps, i.e., κ^1 -bpy ligand loss.

Supplementary Materials: The following are available online at <http://www.mdpi.com/2304-6740/8/2/15/s1>, Figure S1: MO diagram schematizing the interaction between the metallic fragment in the ^3MC state and the approaching acetonitrile ligand; Figure S2: MO diagram at selected points along the reaction path; Cartesian coordinates of the 20 beads along the minimum energy path.

Author Contributions: A.S. performed the research and analyzed the data. I.M.D., F.A. and J.-L.H. conceived and supervised the work, and analyzed the data. I.M.D. wrote the original draft, which F.A. and J.-L.H. reviewed. All authors have read and agreed to the published version of the manuscript.

Funding: This research received no external funding.

Acknowledgments: HPC resources from LCPQ and from CALMIP (p1112 project) are kindly acknowledged.

Conflicts of Interest: The authors declare no conflict of interest.

References

1. Juris, A.; Balzani, V.; Barigelletti, F.; Campagna, S.; Belser, P.; von Zelewsky, A. Ru(II) Polypyridine Complexes: Photophysics, Photochemistry, Electrochemistry, and Chemiluminescence. *Coord. Chem. Rev.* **1988**, *84*, 85–277. [\[CrossRef\]](#)
2. Van Houten, J.; Watts, R.J. Photochemistry of Tris(2,2'-bipyridyl)ruthenium(II) in Aqueous Solution. *Inorg. Chem.* **1978**, *17*, 3381–3385. [\[CrossRef\]](#)
3. Alary, F.; Heully, J.-L.; Bijeire, L.; Vicendo, P. Is the $^3\text{MLCT}$ the Only Photoreactive State of Polypyridyl Complexes? *Inorg. Chem.* **2007**, *46*, 3154–3165. [\[CrossRef\]](#)
4. Alary, F.; Boggio-Pasqua, M.; Heully, J.-L.; Marsden, C.J.; Vicendo, P. Theoretical Characterization of the Lowest Triplet Excited States of the Tris-(1,4,5,8-tetraazaphenanthrene)Ruthenium Dication Complex. *Inorg. Chem.* **2008**, *47*, 5259–5266. [\[CrossRef\]](#)
5. Heully, J.-L.; Alary, F.; Boggio-Pasqua, M. Spin-orbit effects on the photophysical properties of $\text{Ru}(\text{bpy})_3^{2+}$. *J. Chem. Phys.* **2009**, *131*, 184308. [\[CrossRef\]](#)
6. Sanz García, J.; Alary, F.; Boggio-Pasqua, M.; Dixon, I.M.; Heully, J.-L. Is Photoisomerization Required for NO Photorelease in Ruthenium Nitrosyl Complexes? *J. Mol. Model.* **2016**, *22*, 284. [\[CrossRef\]](#)
7. Göttle, A.J.; Alary, F.; Boggio-Pasqua, M.; Dixon, I.M.; Heully, J.-L.; Bahreman, A.; Askes, S.H.C.; Bonnet, S. Pivotal Role of a Pentacoordinate ^3MC State on the Photocleavage Efficiency of a Thioether Ligand in Ruthenium(II) Complexes: A Theoretical Mechanistic Study. *Inorg. Chem.* **2016**, *55*, 4448–4456. [\[CrossRef\]](#)

8. Dixon, I.M.; Heully, J.-L.; Alary, F.; Elliott, P.I.P. Theoretical illumination of highly original photoreactive ^3MC states and the mechanism of the photochemistry of Ru(II) tris(bidentate) complexes. *Phys. Chem. Chem. Phys.* **2017**, *19*, 27765–27778. [[CrossRef](#)]
9. Daniel, C.; Gourlaouen, C. Chemical bonding alteration upon electronic excitation in transition metal complexes. *Coord. Chem. Rev.* **2017**, *344*, 131–149. [[CrossRef](#)]
10. Abrahamsson, M.; Lundqvist, M.J.; Wolpher, H.; Johansson, O.; Eriksson, L.; Bergquist, J.; Rasmussen, T.; Becker, H.-C.; Hammarström, L.; Norrby, P.-O.; et al. Steric Influence on the Excited-State Lifetimes of Ruthenium Complexes with Bipyridyl–Alkanylene–Pyridyl Ligands. *Inorg. Chem.* **2008**, *47*, 3540–3548. [[CrossRef](#)]
11. Borg, O.A.; Godinho, S.S.M.C.; Lundqvist, M.J.; Lunell, S.; Persson, P. Computational Study of the Lowest Triplet State of Ruthenium Polypyridyl Complexes Used in Artificial Photosynthesis. *J. Phys. Chem. A* **2008**, *112*, 4470–4476. [[CrossRef](#)]
12. Österman, T.; Abrahamsson, M.; Becker, H.-C.; Hammarström, L.; Persson, P. Influence of Triplet State Multidimensionality on Excited State Lifetimes of Bis-tridentate Ru(II) Complexes: A Computational Study. *J. Phys. Chem. A* **2012**, *116*, 1041–1050. [[CrossRef](#)]
13. Fredin, L.A.; Wallenstein, J.; Sundin, E.; Jarenmark, M.; Barbosa de Mattos, D.F.; Persson, P.; Abrahamsson, M. Excited State Dynamics of Bistridentate and Trisbidentate Ru(II) Complexes of Quinoline-Pyrazole Ligands. *Inorg. Chem.* **2019**, *58*, 16354–16363. [[CrossRef](#)]
14. Salassa, L.; Garino, C.; Salassa, G.; Gobetto, R.; Nervi, C. Mechanism of Ligand Photodissociation in Photoactivable $[\text{Ru}(\text{bpy})_2\text{L}_2]^{2+}$ Complexes: A Density Functional Theory Study. *J. Am. Chem. Soc.* **2008**, *130*, 9590–9597. [[CrossRef](#)]
15. Salassa, L.; Garino, C.; Salassa, G.; Nervi, C.; Gobetto, R.; Lamberti, C.; Gianolio, D.; Bizzarri, R.; Sadler, P.J. Ligand-Selective Photodissociation from $[\text{Ru}(\text{bpy})(4\text{AP})_4]^{2+}$: A Spectroscopic and Computational Study. *Inorg. Chem.* **2009**, *48*, 1469–1481. [[CrossRef](#)]
16. Borfecchia, E.; Garino, C.; Gianolio, D.; Salassa, L.; Gobetto, R.; Lamberti, C. Monitoring excited state dynamics in *cis*- $[\text{Ru}(\text{bpy})_2(\text{py})_2]^{2+}$ by ultrafast synchrotron techniques. *Catal. Today* **2014**, *229*, 34–45. [[CrossRef](#)]
17. Breivogel, A.; Meister, M.; Förster, C.; Laquai, F.; Heinze, K. Excited State Tuning of Bis(tridentate) Ruthenium(II) Polypyridine Chromophores by Push-Pull Effects and Bite Angle Optimization: A Comprehensive Experimental and Theoretical Study. *Chem. Eur. J.* **2013**, *19*, 13745–13760. [[CrossRef](#)]
18. Kreitner, C.; Heinze, K. Excited state decay of cyclometalated polypyridine ruthenium complexes: Insight from theory and experiment. *Dalton Trans.* **2016**, *45*, 13631–13647. [[CrossRef](#)]
19. Sun, Q.; Mosquera-Vazquez, S.; Lawson Daku, L.M.; Guénée, L.; Goodwin, H.A.; Vauthey, E.; Hauser, A. Experimental Evidence of Ultrafast Quenching of the $^3\text{MLCT}$ Luminescence in Ruthenium(II) Tris-bipyridyl Complexes via a ^3dd State. *J. Am. Chem. Soc.* **2013**, *135*, 13660–13663. [[CrossRef](#)]
20. Sun, Q.; Dereka, B.; Vauthey, E.; Lawson Daku, L.M.; Hauser, A. Ultrafast Transient IR Spectroscopy and DFT Calculations of Ruthenium(II) Polypyridyl Complexes. *Chem. Sci.* **2017**, *8*, 223–230. [[CrossRef](#)]
21. Ding, L.; Chung, L.W.; Morokuma, K. Excited-State Proton Transfer Controls Irreversibility of Photoisomerization in Mononuclear Ruthenium(II) Monoaquo Complexes: A DFT Study. *J. Chem. Theory Comput.* **2014**, *10*, 668–675. [[CrossRef](#)]
22. Greenough, S.E.; Roberts, G.M.; Smith, N.A.; Horbury, M.D.; McKinlay, R.G.; Žurek, J.M.; Paterson, M.J.; Sadler, P.J.; Stavros, V.G. Ultrafast photo-induced ligand solvolysis of *cis*- $[\text{Ru}(\text{bipyridine})_2(\text{nicotinamide})_2]^{2+}$: Experimental and theoretical insight into its photoactivation mechanism. *Phys. Chem. Chem. Phys.* **2014**, *16*, 19141–19155. [[CrossRef](#)]
23. Camilo, M.R.; Cardoso, C.R.; Carlos, R.M.; Lever, A.B.P. Photosolvolysis of *cis*- $[\text{Ru}(\alpha\text{-diimine})_2(4\text{-aminopyridine})_2]^{2+}$ Complexes: Photophysical, Spectroscopic, and Density Functional Theory Analysis. *Inorg. Chem.* **2014**, *53*, 3694–3708. [[CrossRef](#)]
24. Tu, Y.-J.; Mazumder, S.; Endicott, J.F.; Turro, C.; Kodanko, J.J.; Schlegel, H.B. Selective Photodissociation of Acetonitrile Ligands in Ruthenium Polypyridyl Complexes Studied by Density Functional Theory. *Inorg. Chem.* **2015**, *54*, 8003–8011. [[CrossRef](#)]
25. Nisbett, K.; Tu, Y.-J.; Turro, C.; Kodanko, J.J.; Schlegel, H.B. DFT Investigation of Ligand Photodissociation in $[\text{Ru}(\text{II})(\text{tpy})(\text{bpy})(\text{py})]^{2+}$ and $[\text{Ru}(\text{II})(\text{tpy})(\text{Me}_2\text{bpy})(\text{py})]^{2+}$ Complexes. *Inorg. Chem.* **2018**, *57*, 231–240. [[CrossRef](#)]

26. Petroni, A.; Slep, L.D.; Etchenique, R. Ruthenium(II) 2,2'-Bipyridyl Tetrakis Acetonitrile Undergoes Selective Axial Photocleavage. *Inorg. Chem.* **2008**, *47*, 951–956. [\[CrossRef\]](#)
27. Rojas Pérez, Y.; Slep, L.D.; Etchenique, R. *Cis-Trans* Interconversion in Ruthenium(II) Bipyridine Complexes. *Inorg. Chem.* **2019**, *58*, 11606–11613. [\[CrossRef\]](#)
28. Feng, L.; Wang, Y.; Jia, J. Triplet Ground-State-Bridged Photochemical Process: Understanding the Photoinduced Chiral Inversion at the Metal Center of $[\text{Ru}(\text{phen})_2(\text{l-ser})]^+$ and Its Bipy Analogues. *Inorg. Chem.* **2017**, *56*, 14467–14476. [\[CrossRef\]](#)
29. Jacquemin, D.; Escudero, D. The Short Device Lifetimes of Blue PhOLEDs: Insights into the Photostability of Blue Ir(III) Complexes. *Chem. Sci.* **2017**, *8*, 7844–7850. [\[CrossRef\]](#)
30. Arroliga-Rocha, S.; Escudero, D. Facial and Meridional Isomers of Tris(bidentate) Ir(III) Complexes: Unravelling Their Different Excited State Reactivity. *Inorg. Chem.* **2018**, *57*, 12106–12112. [\[CrossRef\]](#)
31. Escudero, D. *Mer-Ir(ppy)₃* to *Fac-Ir(ppy)₃* Photoisomerization. *ChemPhotoChem* **2019**, *3*, 697–701. [\[CrossRef\]](#)
32. Göttle, A.J.; Dixon, I.M.; Alary, F.; Heully, J.-L.; Boggio-Pasqua, M. Adiabatic Versus Nonadiabatic Photoisomerization in Photochromic Ruthenium Sulfoxide Complexes: A Mechanistic Picture from Density Functional Theory Calculations. *J. Am. Chem. Soc.* **2011**, *133*, 9172–9174. [\[CrossRef\]](#)
33. Göttle, A.J.; Alary, F.; Dixon, I.M.; Heully, J.-L.; Boggio-Pasqua, M. Unravelling the S→O Linkage Photoisomerization Mechanisms in *cis*- and *trans*- $[\text{Ru}(\text{bpy})_2(\text{DMSO})_2]^{2+}$ Using Density Functional Theory. *Inorg. Chem.* **2014**, *53*, 6752–6760. [\[CrossRef\]](#)
34. Sanz García, J.; Alary, F.; Boggio-Pasqua, M.; Dixon, I.M.; Malfant, I.; Heully, J.-L. Establishing the Two-Photon Linkage Isomerization Mechanism in the Nitrosyl Complex *trans*- $[\text{RuCl}(\text{NO})(\text{py})_4]^{2+}$ by DFT and TDDFT. *Inorg. Chem.* **2015**, *54*, 8310–8318. [\[CrossRef\]](#)
35. Lebon, E.; Bastin, S.; Sutra, P.; Vendier, L.; Piau, R.E.; Dixon, I.M.; Boggio-Pasqua, M.; Alary, F.; Heully, J.-L.; Igau, A.; et al. Can a Functionalized Phosphine Ligand Promote Room Temperature Luminescence of the $[\text{Ru}(\text{bpy})(\text{tpy})]^{2+}$ Core? *Chem. Commun.* **2012**, *48*, 741–743. [\[CrossRef\]](#)
36. Triadon, A.; Grelaud, G.; Richy, N.; Mongin, O.; Moxey, G.J.; Dixon, I.M.; Yang, X.; Wang, G.; Barlow, A.; Rault-Berthelot, J.; et al. Linear and Third-Order Nonlinear Optical Properties of $\text{Fe}(\eta^5\text{-C}_5\text{Me}_5)(\kappa^2\text{-dppe})$ - and *trans*- $\text{Ru}(\kappa^2\text{-dppe})_2$ -Alkynyl Complexes Containing 2-Fluorenyl End Groups. *Organometallics* **2018**, *37*, 2245–2262. [\[CrossRef\]](#)
37. Guillon, T.; Boggio-Pasqua, M.; Alary, F.; Heully, J.-L.; Lebon, E.; Sutra, P.; Igau, A. Theoretical Investigation on the Photophysical Properties of Model Ruthenium Complexes with Diazabutadiene Ligands $[\text{Ru}(\text{bpy})_{3-x}(\text{dab})_x]^{2+}$ ($x = 1\text{--}3$). *Inorg. Chem.* **2010**, *49*, 8862–8872. [\[CrossRef\]](#)
38. Vieuxmaire, O.P.J.; Piau, R.E.; Alary, F.; Heully, J.-L.; Sutra, P.; Igau, A.; Boggio-Pasqua, M. Theoretical Investigation of Phosphinidene Oxide Polypyridine Ruthenium(II) Complexes: Toward the Design of a New Class of Photochromic Compounds. *J. Phys. Chem. A* **2013**, *117*, 12821–12830. [\[CrossRef\]](#)
39. Dixon, I.M.; Alary, F.; Boggio-Pasqua, M.; Heully, J.-L. The $(\text{N}_4\text{C}_2)^{2-}$ Donor Set as Promising Motif for Bis(tridentate) Iron(II) Photoactive Compounds. *Inorg. Chem.* **2013**, *52*, 13369–13374. [\[CrossRef\]](#)
40. Dixon, I.M.; Khan, S.; Alary, F.; Boggio-Pasqua, M.; Heully, J.-L. Probing the photophysical capability of mono and bis(cyclometallated) Fe(II) polypyridine complexes using inexpensive ground state DFT. *Dalton Trans.* **2014**, *43*, 15898–15905. [\[CrossRef\]](#)
41. Dixon, I.M.; Alary, F.; Boggio-Pasqua, M.; Heully, J.-L. Reversing the relative $^3\text{MLCT}$ - ^3MC order in Fe(II) complexes using cyclometallating ligands: A computational study aiming at luminescent Fe(II) complexes. *Dalton Trans.* **2015**, *44*, 13498–13503. [\[CrossRef\]](#)
42. Dixon, I.M.; Boissard, G.; Whyte, H.; Alary, F.; Heully, J.-L. Computational Estimate of the Photophysical Capabilities of Four Series of Organometallic Iron(II) Complexes. *Inorg. Chem.* **2016**, *55*, 5089–5091. [\[CrossRef\]](#)
43. Durham, B.; Caspar, J.V.; Nagle, J.K.; Meyer, T.J. Photochemistry of $\text{Ru}(\text{bpy})_3^{2+}$. *J. Am. Chem. Soc.* **1982**, *104*, 4803–4810. [\[CrossRef\]](#)
44. Kirchhoff, J.R.; McMillin, D.R.; Marnot, P.A.; Sauvage, J.-P. Photochemistry and Photophysics of Bis(terpyridyl) Complexes of Ru(II) in Fluid Solution. Evidence for the Formation of an η^2 -Diphenylterpyridine Complex. *J. Am. Chem. Soc.* **1985**, *107*, 1138–1141. [\[CrossRef\]](#)
45. Thompson, D.W.; Wishart, J.F.; Brunschwig, B.S.; Sutin, N. Efficient Generation of the Ligand Field Excited State of Tris-(2,2'-bipyridine)-ruthenium(II) through Sequential Two-Photon Capture by $[\text{Ru}(\text{bpy})_3]^{2+}$ or Electron Capture by $[\text{Ru}(\text{bpy})_3]^{3+}$. *J. Phys. Chem. A* **2001**, *105*, 8117–8122. [\[CrossRef\]](#)

46. Kunnus, K.; Josefsson, I.; Rajkovic, I.; Schreck, S.; Quevedo, W.; Beye, M.; Weniger, C.; Grübel, S.; Scholz, M.; Nordlund, D.; et al. Identification of the dominant photochemical pathways and mechanistic insights to the ultrafast ligand exchange of $\text{Fe}(\text{CO})_5$ to $\text{Fe}(\text{CO})_4\text{EtOH}$. *Struct. Dyn.* **2016**, *3*, 043204. [\[CrossRef\]](#)
47. Reinhard, M.; Auböck, G.; Besley, N.A.; Clark, I.P.; Greetham, G.M.; Hanson-Heine, M.W.D.; Horvath, R.; Murphy, T.S.; Penfold, T.J.; Towrie, M.; et al. Photoaquation Mechanism of Hexacyanoferrate(II) Ions: Ultrafast 2D UV and Transient Visible and IR Spectroscopies. *J. Am. Chem. Soc.* **2017**, *139*, 7335–7347. [\[CrossRef\]](#)
48. Welby, C.E.; Rice, C.R.; Elliott, P.I.P. Unambiguous Characterization of a Photoreactive Ligand-Loss Intermediate. *Angew. Chem. Int. Ed.* **2013**, *52*, 10826–10829. [\[CrossRef\]](#)
49. Welby, C.E.; Armitage, G.K.; Bartley, H.; Wilkinson, A.; Sinopoli, A.; Uppal, B.S.; Rice, C.R.; Elliott, P.I.P. Photochemistry of Ru(II) 4,4'-Bi-1,2,3-triazolyl (btz) Complexes: Crystallographic Characterization of the Photoreactive Ligand-Loss Intermediate *trans*-[Ru(bpy)(κ^2 -btz)(κ^1 -btz)(NCMe)]²⁺. *Chem. Eur. J.* **2014**, *20*, 8467–8476. [\[CrossRef\]](#)
50. Soupart, A.; Alary, F.; Heully, J.-L.; Elliott, P.I.P.; Dixon, I.M. Exploration of Uncharted ³PES Territory for [Ru(bpy)₃]²⁺: A New ³MC Minimum Prone to Ligand Loss Photochemistry. *Inorg. Chem.* **2018**, *57*, 3192–3196. [\[CrossRef\]](#)
51. Jónsson, H.; Mills, G.; Jacobsen, K.W. Nudged elastic band method for finding minimum energy paths of transitions. In *Classical and Quantum Dynamics in Condensed Phase Simulations*; Berne, B.J., Cicotti, G., Coker, D.F., Eds.; World Scientific: Singapore, 1998; pp. 385–404.
52. Henkelman, G.; Johansson, G.; Jónsson, H. Methods for Finding Saddle Points and Minimum Energy Paths. In *Progress on Theoretical Chemistry and Physics*; Schwartz, S.D., Ed.; Kluwer Academic: Dordrecht, The Netherlands, 2000; pp. 269–302.
53. Smidstrup, S.; Pedersen, A.; Stokbro, K.; Jónsson, H. Improved initial guess for minimum energy path calculations. *J. Chem. Phys.* **2014**, *140*, 214106. [\[CrossRef\]](#)
54. Soupart, A.; Alary, F.; Heully, J.-L.; Elliott, P.I.P.; Dixon, I.M. Recent Progress in Ligand Photorelease Reaction Mechanisms: Theoretical Insights Focusing on Ru(II) ³MC States. *Coord. Chem. Rev.* **2020**, *408*, 213184. [\[CrossRef\]](#)
55. Neese, F. The ORCA Program System. *Wiley Interdiscip. Rev. Comput. Mol. Sci.* **2012**, *2*, 73–78. [\[CrossRef\]](#)
56. Lee, C.; Yang, W.; Parr, R.G. Development of the Colle-Salvetti Correlation-Energy Formula into a Functional of the Electron Density. *Phys. Rev. B* **1988**, *37*, 785–789. [\[CrossRef\]](#)
57. Becke, A.D. Density-functional thermochemistry. III. The role of exact exchange. *J. Chem. Phys.* **1993**, *98*, 5648–5652. [\[CrossRef\]](#)
58. Andrae, D.; Haeussermann, U.; Dolg, M.; Stoll, H.; Preuss, H. Energy-adjusted ab initio Pseudopotentials for the Second and Third Row Transition Elements. *Theor. Chim. Acta* **1990**, *77*, 123–141. [\[CrossRef\]](#)
59. Weigend, F.; Ahlrichs, R. Balanced Basis Sets of Split Valence, Triple Zeta Valence and Quadruple Zeta Valence Quality for H to Rn: Design and Assessment of Accuracy. *Phys. Chem. Chem. Phys.* **2005**, *7*, 3297–3305. [\[CrossRef\]](#)
60. Grimme, S.; Antony, J.; Ehrlich, S.; Krieg, H. A Consistent and Accurate ab initio Parametrization of Density Functional Dispersion Correction (DFT-D) for the 94 Elements H-Pu. *J. Chem. Phys.* **2010**, *132*, 154104. [\[CrossRef\]](#)
61. Grimme, S.; Ehrlich, S.; Goerigk, L. Effect of the Damping Function in Dispersion Corrected Density Functional Theory. *J. Comput. Chem.* **2011**, *32*, 1456–1465. [\[CrossRef\]](#)
62. Marenich, A.V.; Cramer, C.J.; Truhlar, D.G. Universal Solvation Model Based on Solute Electron Density and on a Continuum Model of the Solvent Defined by the Bulk Dielectric Constant and Atomic Surface Tensions. *J. Phys. Chem. B* **2009**, *113*, 6378–6396. [\[CrossRef\]](#)
63. Allouche, A.-R. Gabedit-A Graphical User Interface for Computational Chemistry Softwares. *J. Comput. Chem.* **2011**, *32*, 174–182. [\[CrossRef\]](#)
64. Herbol, H.C.; Stevenson, J.; Clancy, P. Computational Implementation of Nudged Elastic Band, Rigid Rotation, and Corresponding Force Optimization. *J. Chem. Theory Comput.* **2017**, *13*, 3250–3259. [\[CrossRef\]](#)

